Research article

polymers advanced technologies

Received: 10 March 2013, Revised: 15 May 2013, Accepted: 21 May 2013, Published online in Wiley Online Library: 24 June 2013

(wileyonlinelibrary.com) DOI: 10.1002/pat.3161

Microstructure and anti- wear and corrosion performances of novel UHMWPE/graphene-nanosheet composite coatings deposited by flame spraying

Jing Han[a,b], Siyue Ding[a], Wenge Zheng[c], Wenya Li[b] and Hua Li[a]*

Ultra-high molecular weight polyethylene (UHMWPE)/graphene-nanosheet (GN, multiple layers of graphene sheets with the thickness of ~5–10 nm) coatings have been deposited by flame spraying. The structure of UHMWPE remained almost intact after the spray processing and addition of GNs resulted in a slightly decreased crystallinity and improved thermal stability of UHMWPE. In addition, the coating containing 1.0 wt.% GNs exhibited a reduction of ~20% in wear rate and 25% in friction coefficient (0.18 *versus* 0.24). Significantly enhanced anti-corrosion performances of the UHMWPE–GN coatings were suggested by increased corrosion potential, corrosion current density, and impedance modulus value of the UHMWPE–GN coatings. The very well retained GNs are located mainly at the interfaces between UHMWPE splats and act as bridges connecting the splats, which mainly accounts for the enhanced properties of the composite coatings. The novel UHMWPE–graphene composite coatings show great potential for protecting engineering components for applications against corrosion. Copyright © 2013 John Wiley & Sons, Ltd.

Keywords: UHMWPE; graphene; corrosion; wear; composite coating

INTRODUCTION

Due to its favorable biocompatibility, strong strength, high fatigue, and wear resistance, ultra-high molecular weight polyethylene (UHMWPE) has been widely used since it was first introduced in 1962.[1] In spite of its excellent mechanical properties, however, the application of UHMWPE is restricted due to poor processability attributed to its high viscosity.[2] Extensive efforts have therefore been paid to modify the structure of UHMWPE. Various approaches have been developed, among which incorporation of other materials leads the related research. Cross-linking,[3,4] self-reinforcement with UHMWPE fibers,[5] reinforcement by carbon fibers[6] and nanoparticles[7] and carbon nanotubes,[2,8,9] modification by oxygen plasma,[10] and other UHMWPE-based composites[11] have shown promising strengthening effect. Emergence of graphene nanosheet (GN), defined here as multiple graphene sheets with the thickness of less than 10 nm, has recently opened up an exciting new field in the science and technology of two-dimensional nanomaterials for its unique structure and enhanced properties. In the past few years, attempts have been made by worldwide researchers to address the effect of addition of graphene platelets on mechanical properties of polymer-based composites. GN-based materials have enormous potential to rival or even surpass the performance of carbon nanotube-based counterparts. Previous research efforts have evidenced that the loading of 1.0 wt.% graphene oxide nanosheets into UHMWPE resulted in significant improvement in both microhardness and anti-wear resistance with alteration of tribological behavior from fatigue to abrasive.[12] By complete exfoliation of graphite, molecular-level dispersion of chemically modified individual GNs within polymer hosts has been achieved.[13] However, fabrication of UHMWPE and UHMWPE-based composites in the form of films/coatings remains challenging yet. In recent years, polymer composites have found extensive applications in micro-electromechanical systems as corrosion protective coatings, bioactive coatings, and biomedical scaffolds.[2] Flame spray technique has been developing rapidly in recent decades and was believed to be one of the most appropriate approaches for depositing polymer coatings.[14] Coatings of polyethylene-terephthalate,[15,16] UHMWPE and UHMWPE–EAA composites,[2] poly-ethereetherketone [17,18], and polypropylene[19] with favorable adhesion and ductility have been successfully fabricated by flame spray. Thermal sprayed coatings with desirable adhesion and other mechanical properties provide a cost-effective way to protect and prolong the lifespan of not only steel components but many other substrates used within engineering applications. As the core subject for thermal spray

* *Correspondence to: Hua Li, Division of Surface Engineering, Ningbo Institute of Materials Technology and Engineering, Chinese Academy of Sciences, Ningbo 315201, China.*
E-mail: lihua@nimte.ac.cn

a *J. Han, S. Ding, H. Li*
Division of Surface Engineering, Ningbo Institute of Materials Technology and Engineering, Chinese Academy of Sciences, Ningbo 315201, China

b *J. Han, W. Li*
State Key Laboratory of Solidification Processing, Northwestern Polytechnical University, Xian 710072, China

c *W. Zheng*
Ningbo Key Laboratory of Polymer Materials, Ningbo Institute of Materials Technology and Engineering, Chinese Academy of Sciences, Ningbo 315201, China

community, appropriate structure and advanced properties of polymer coatings are expected by addition of other materials, among which GNs are an attractive candidate.

In this study, UHMWPE and GN (multiple graphene sheets with the thickness of less than 10 nm)-reinforced UHMWPE coatings were deposited on 304 L substrates by flame spray technique. Characterization of microstructure and evaluation of mechanical properties in terms of anti-wear and corrosion performances of the coatings were conducted, and the relationship between microstructure and properties was elucidated.

MATERIALS AND METHODS

Materials

Commercial UHMWPE powders (density: 930 kg/m^3, Nantong Yangba Polyethylene Co., Ltd., China) were sieved to attain the sprayable particle size range of $-120+80$ μm. Graphene was made by stripping of graphite oxide through high-temperature expansion. Preparation of the graphite oxide was fabricated according to the Staudenmaier method as described elsewhere.[20] For deposition of UHMWPE–GN composite coatings, the starting UHMWPE feedstock powders were mechanically blended with GNs of 0.15 wt.%, 0.3 wt.%, and 1.0 wt.%. The mixture was homogenized with ethanol and deionized water being used as cooling medium by ball-milling at 300 rpm for 6 h. Drying was then conducted in a blast oven at 60°C. Typical morphology of the powders is shown in Fig. 1. Near-spherical shape is seen for the UHMWPE particles (Fig. 1a), and graphene in multiple layers has been entirely embedded in UHMWPE particles (Fig. 1b). The thickness of the GN was less than 10 nm, as shown in the enlarged view in Fig. 1b. It is clear that the multi-layered graphene is evenly distributed in individual UHMWPE particles. Raman spectrum of the GNs was also shown in Fig. 1b, indicating exclusive presence of the synthesized GNs used in this study.

Coating deposition

The UHMWPE and UHMWPE-GN coatings were deposited by flame spraying the powders onto 304 L stainless steel substrates with the dimension of 2 cm × 4 cm × 0.2 cm in width, length, and thickness, respectively. Prior to the spraying, the substrates were sonication cleaned in acetone and subsequently grit blasted. For the coating deposition, the substrates were preheated to 110–130°C by a hot plate, and the temperature was measured by infrared thermometer (ST60, Raylek). The flame spray used FS-4 multi-functional powder flame spray torch and employed acetylene as the fuel gas and oxygen as the oxidant. The pressure and flow rate of oxygen and acetylene were fixed at 0.3 MPa, 0.25 m^3/h, and 0.1 MPa, 0.30 m^3/h, respectively. Compressed air was also used for the spraying, and the pressure and flow rate were 0.4 MPa and 3–5 m^3/h, respectively. The powder feeding rate was 15 g/min, and the spray distance was 250 mm.

Microstructure characterization and property assessment

Microstructure of the powders and coatings was characterized by field emission scanning electron microscopy (FESEM, Quanta FEG 250, FEI). Vickers hardness of the coatings was measured on their polished cross sections using the HV-1000 microhardness tester with a load of 0.25 N and the duration of 10 s. A total of at least ten points were averaged for each sample. The tribological properties of the coatings were assessed by sliding wear test conducted on a reciprocating-type ball-on-disc tribometer (UMT-3, USA). The initial maximum Hertzian contact pressure was 91.83 MPa. The tests were performed for 1800 s at room temperature under a load of 35 N with an average sliding speed of 10 mm/s. 304 L stainless steel balls with the size of 9.5 mm in diameter were used as the counterparts. Prior to each test, the 304 balls were ultrasonically cleaned in acetone, and a new ball or a new position of the ball was adopted for each test. Five samples were tested for each type of the coatings. The friction coefficient as the function of sliding time was recorded during the test. After the test, wear loss in terms of wear volume was determined using a three-dimensional surface profiler (Alpha-Step IQ, USA), and the wear rate was also calculated. Morphological features of the worn surfaces were examined by FESEM observation. In addition, to evaluate the influence of GNs on structure stability and crystallization behavior of UHMWPE, thermogravimetric analysis (TGA, Pyris Diamond TG/DTA, Perkin-Elmer, USA) and differential scanning calorimetry testing (DSC, Pyris Diamond DSC, Perkin-Elmer, USA) were conducted for the samples. Nitrogen gas with a flow rate of 200 ml/min was used for the TGA test, and the temperature range was 30–600°C with a heating rate of 10°C/min. For the DSC test in nitrogen atmosphere, the heating rate of the samples was 10°C/min. Phases in the powders and coatings were detected by X-ray diffraction (XRD, Bruker AXS, Germany) performed at a scanning rate of 0.1°/s using monochromatic Cu-K_α radiation operated at 40 kV. The XRD results were further analyzed by Jade software equipped with the instrument. Furthermore, chemical modifications of UHMWPE due to the high-temperature spray processing were investigated by Fourier transform infrared spectroscopy (FTIR, NICOLET6700, Thermal Fisher Scientific, USA). Electrochemical corrosion behavior of the UHMWPE–GN composite coatings were evaluated by potentiodynamic polarization test and electrochemical impedance spectroscopy (EIS) measurement utilizing a PGSTAT 302 autolab electrochemical workstation in a saline solution of 3.5 wt.% NaCl. A three-electrode cell was used. The working electrode was a bare substrate or a coated one with an exposed area of 0.15 cm^2. A saturated calomel electrode was used as the reference electrode to measure the potential across the electrochemical interface, and a platinum sheet (20 mm × 10 mm) was employed as the auxiliary electrode. The polarization curves were obtained by sweeping the potential from the cathode to the anode at a rate of 2 mVs^{-1}. Corrosion current density values were calculated from potentiodynamic polarization tests. Impedance spectra were obtained in the frequency range of 100 kHz–0.01 Hz with the amplitude of the sinusoidal perturbation applied to the electrode being 10 mV. The impedance curves were simulated by using the software FRA equipped with the workstation.

RESULTS AND DISCUSSION

Microstructure of the coatings

Dense microstructure for all the UHMWPE and UHMWPE–GN coatings has been achieved, as typically shown in Fig. 1. Apart from the absence of cracks or other superficial defects, no visible pores or inclusions are noticed in the coatings (Fig. 1c,d), presumably indicating feasibility of the flame spray for depositing UHMWPE-based coatings. Typical topographical view

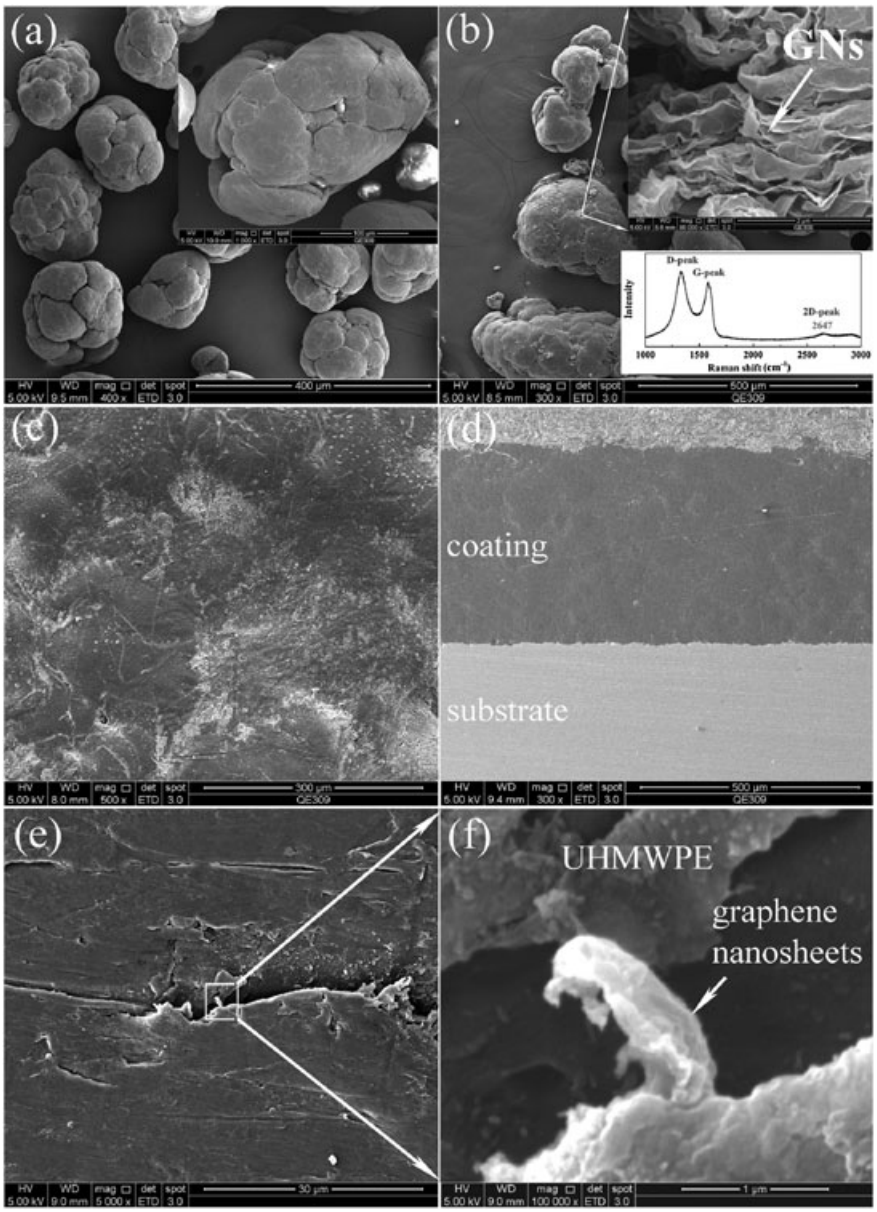

Figure 1. Typical FESEM morphology of the powders and coatings, (a) FESEM images of the starting UHMWPE powders and (b) the UHMWPE–1.0wt.% GN powders, embedding of GNs in UHMWPE particles can be clearly seen from the closer view, and Raman spectrum of the GNs was also shown, indicating exclusive presence of the synthesized GNs used in this study; (c,d) SEM images of the typical UHMWPE–GN coatings taken from their surfaces (c) and cross sections (d) showing their dense structure and smooth surface; and (e,f) FESEM images of the UHMWPE–1.0wt.%GN coating showing that graphene in the form of multiple sheets with the thickness of ~5–10 nm is predominately located at UHMWPE splats' interfaces.

of the coating (Fig. 1c) further clearly suggests well melt state of the UHMWPE particles during the spraying, which is mainly responsible for the unidentifiable splats' interfaces. Close cross-sectional examination of manually fractured UHMWPE–1wt.%GN coating shows well-retained graphene sheets in the coatings (Fig. 1e,f). It is noted that GNs are located mainly at the interfaces between UHMWPE splats and act as bridges connecting the splats. The thickness of the GNs is in a range of ~5–10 nm. XRD detection shows typical feature of UHMWPE, while the peaks for GNs are not detectable (Fig. 2). The flame spraying did not bring about marked changes in chemistry of UHMWPE. However, it is noted that compared to the starting feedstock powders, there is remarkable increase in relative intensity of the peaks referring to (110) and (200) planes in the coatings. The increase in peak magnitude for the (110) plane is the most noticeable, indicating the most significant growth of the crystallites along the [110] direction. The current flame spray processing, which involves melting and solidification of UHMWPE, together with the addition of GNs, has slightly altered the crystallization behavior of UHMWPE.

To further elucidate the effect of the addition of GNs on the crystallization behavior of UHMWPE, DSC test was conducted for both the UHMWPE–GN powders and coatings. As shown in Fig. 3a, the mechanically mixed GNs in UHMWPE had minor influence on the crystallization temperature of UHMWPE. For the coatings, surprisingly, it is noted that the addition of 1.0 wt.% GNs delayed the crystallization of UHMWPE from 131.4°C to 133.4°C, as suggested by the shifting of the exothermic peaks. This effect does not pertain to the content of GNs in the coatings. In other words,

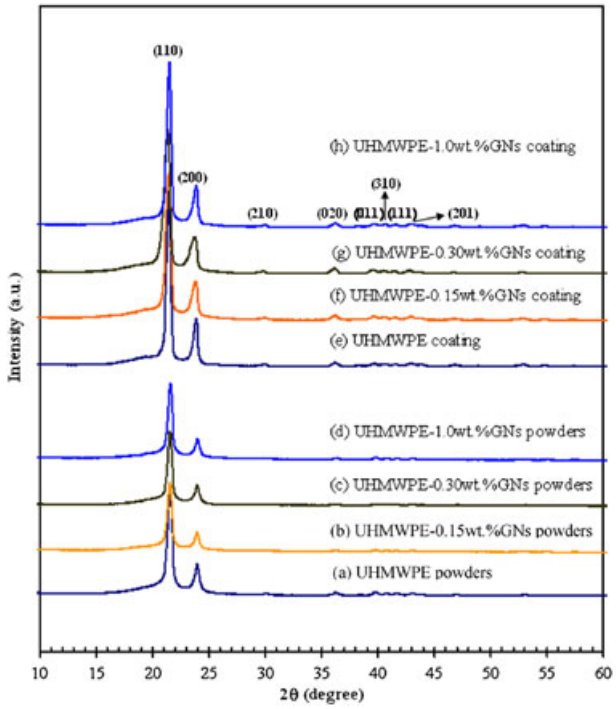

Figure 2. XRD patterns of the UHMWPE and UHMWPE–GN powders and coatings.

presence instead of changes in content of GNs in the powders/coatings affects crystallization behavior of UHMWPE. The difference in crystallization temperature of the pure UHMWPE coating, 131.4°C, from that of the starting feedstock powders, 141.7°C, could be well explained by the fact that crystallization temperature in DSC testing of thermoplastic materials is very dependent on their thermal history.[21] This nevertheless indicates that the thermal property of the flame-sprayed UHMWPE–GN composite coatings was inferior to the powder samples, which may be due to the degradation of UHMWPE during the spraying. Furthermore, based on the DSC curves, the melting temperature (T_m), crystallization enthalpy (ΔH_c), heat of fusion (ΔH_f), and crystallinity (X_C) of the samples were obtained. The crystallinity of the samples was calculated from the endothermic peak according to the following relationship:

$$X_c = \Delta H_f / \Delta H_c \times 100\%. \quad (1)$$

A value of 289.6 J/g[22] for ΔH_C was taken for 100% crystalline UHMWPE. The crystallinity for each sample as calculated by eqn (1) was also shown in Fig. 3a. There is a notable drop in crystallinity in the pure UHMWPE coating compared to the powders (50.3% *versus* 60.2%), which is likely attributed to the rapid cooling of UHMWPE droplets upon impingement on the substrate/precoating during coating formation. In addition, the addition of GNs results in a slight decrease in the crystallinity of UHMWPE. These results are in agreement with the UHMWPP composites filled with the admixture of other carbon fillers like multi-wall carbon nanotubes.[21] The degree of crystallization was observed to increase in exfoliated graphene/PVA,[23] while no effect was observed in graphite-oxide/PVA.[24] Interestingly, however, complete opposite effect was observed in chemically reduced graphite-oxide/PVA that decreased crystallinity was reported.[25] In our case, the decreased crystallinity brought about by addition of GNs is likely caused by multiple factors, which include the nature of polymer crystallization as it is heavily influenced by thermal history, the spray process that was employed, and the interfacial interaction initiated by the fillers.[26]

FTIR characterization of the powder and coating samples gives further knowledge about the effect of GN addition on chemistry of UHMWPE. As shown in Fig. 3b, all the samples exhibit C–H related absorption peaks at 2920, 2850, 1465, and 723 cm^{-1}, which correspond to methylene anti-symmetric stretching vibration, methylene symmetric stretching vibration, methylene changing angle vibration, and methylene rocking vibration, respectively.[27] The absorption peak at 3459 cm^{-1} is probably attributed to the hydroxyl group (–OH) or water absorbed in the samples. The band labeled at ~2350 cm^{-1} presents the carbon dioxide absorption peak, which may contain C = O stretch absorption located in the range of 1750–1600 cm^{-1}.[28] This is most likely due to the reaction of a small amount of UHMWPE

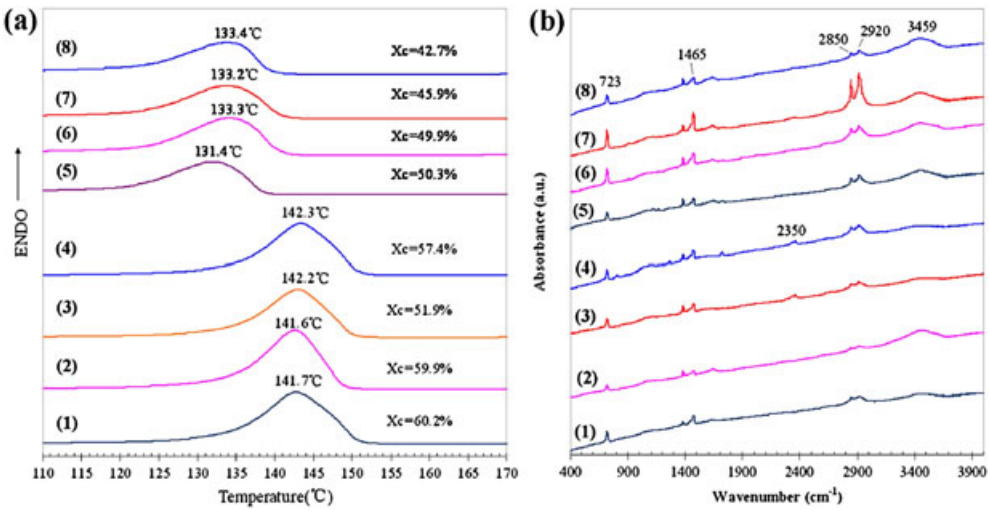

Figure 3. DSC heating curves (a) and FTIR spectra (b) of the powders and coatings, (1) the UHMWPE powders, (2) the UHMWPE–0.15wt.%GN powders, (3) the UHMWPE–0.30wt.%GN powders, (4) the UHMWPE–1.0wt.%GN powders, (5) the UHMWPE coating, (6) the UHMWPE–0.15wt.%GN coating, (7) the UHMWPE–0.30wt.%GN coating, and (8) the UHMWPE–1.0wt.%GN coating. The crystallinity (X_C) of the samples is also shown in (a).

with oxygen in air during sample preparation. It is noted that the FTIR spectra showed no major changes or shifting of the principal peaks for the starting powders and the as-sprayed coatings, evidencing that UHMWPE did not suffer obvious thermal degradation during the coating formation, in spite of the observed changes in their crystalline structure, as suggested by the XRD and DSC analyses. Thermal stability of the powders/coatings was further examined by TG analysis. Minor differences are seen (TG curves not shown). The onset decomposition temperature (T_{od}) of the samples is listed in Table 1. It is clear that T_{od} of the UHMWPE/GN composite powders is slightly higher than that of the pure UHMWPE powders, indicating enhanced thermal stability achieved by addition of GNs. It was reported that hydrogen bonding between graphene oxide and polymer has been responsible for changed thermal behavior.[25] In this study, the improvement in thermal stability of the composite powders should also be partially attributed to the homogeneous distribution of GNs in the UHMWPE matrix (Fig. 1b). The GNs with high aspect ratio may act as a barrier inhibiting the emission of small gaseous molecules.[29] Compared to the powders, the as-sprayed coatings exhibit relatively lower T_{od} values, suggesting that the flame spraying process exerted certain effect on distribution of GNs in the coatings.

Mechanical properties of the coatings

In this study, the UHMWPE–GN coatings were developed primarily for anti-corrosion applications with favorable anti-wear and other mechanical performances. Microhardness, anti-wear performances, and corrosion resistance of the coatings were therefore evaluated. Figure 4 shows the microhardness values of the GN/UHMWPE composite coatings with different GN contents. It can be found that the microhardness of the coatings increases gradually with increase in content of GNs, 6.34Hv for the pure UHMWPE coaing, 6.56Hv for the UHMWPE–0.15wt.%GN coating, 6.95Hv for the UHMWPE–0.3wt.%GN coating, and 7.32Hv for the UHMWPE–1.0wt.%GN coating. The relatively uniform distribution of GNs in the UHMWPE matrix as revealed by FESEM characterization should account for the increased microhardness values, which is likely attributed to intrinsic feature of graphene. However, it is also noted that for the UHMWPE–GN coatings, the deviation of microhardness data is large, indicating incomplete dispersion of GNs in UHMWPE. The wear tests of the coatings showed that addition of GNs brought about marked decrease in friction coefficient, from ~0.24 for the pure UHMWPE coating to ~0.21 for the UHMWPE–0.15wt%GN coating, ~0.19 for the UHMWPE–0.30wt% GN coating, and ~0.18 for the UHMWPE–1.0wt%GN coating (Fig. 5a). While the bare 304 L substrate without surface sand-blasting exhibited an average friction coefficient of 0.65. The wear rate follows the same tendency that increase in GN content gave rise to reduced wear rate (Fig. 5b), suggesting enhanced anti-wear

Table 1. Onset decomposition temperature (T_{od}) of the UHMWPE/GN composite powders and coatings

	Powders (T_{od}/°C)	Coating (T_{od}/°C)
UHMWPE	466.82	460.11
UHMWPE/0.15wt.%GNs	467.88	458.87
UHMWPE/0.3wt.%GNs	469.77	462.42
UHMWPE/1.0wt.%GNs	468.17	464.02

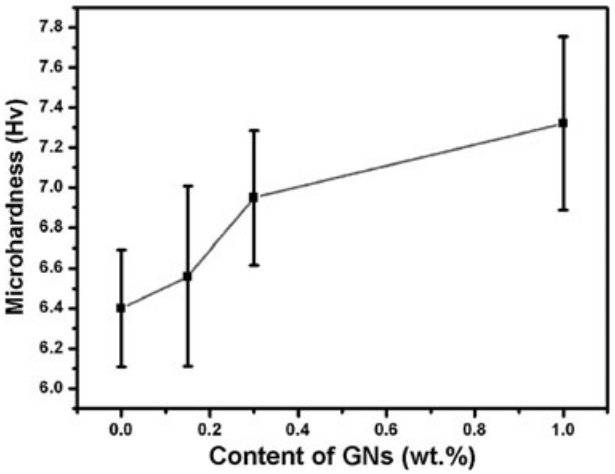

Figure 4. Microhardness of the UHMWPE-based coatings *versus* content of GNs in the coatings.

performances attained by addition of GNs in UHMWPE. The high standard deviation demonstrated by the wear rate might also be attributed to the limited amount and incomplete dispersion of GNs at the surfaces of the coatings. As the GN load is 1.0 wt.%, the reduction of the wear rate is ~20%, indicating an efficient ability of GNs to improve the wear resistance of the polymer matrix at a relatively low loading. It was believed that nanoparticle fillers have been a part of notable reductions in wear rate of polymer matrix at very low loadings.[30] Graphene is basically naturally occurring carbon material; super lubricant property of graphene has therefore been expected, which might favor the enhanced anti-wear behavior of the coatings. In addition, it was found in this study that the presence of GNs in the UHMWPE-based composite coatings showed capability of inhibiting effectively propagation of the cracks induced by indentation (data not shown), which should be attributed mainly to the bridging effect achieved by GNs through their predominant presence at splats' interfaces. This in turn gives clear insight into the most likely strengthening mechanism that GNs play roles in stress transfer and lubrication during wear of the GN-containing UHMWPE coatings. Moreover, the changes in microstructure and chemistry of UHMWPE triggered by the addition of GNs have been revealed previously, e.g. enhanced thermal stability, decreased crystallinity (Fig. 2), etc. SEM observation of the wear scars of the pure UHMWPE coating with a crystallinity of 50.3% shows clearly the wear debris on its surface (Fig. 5c). While the UHMWPE–1.0wt.%GN coating with the crystallinity of 42.7% exhibits the wear scar with obvious plastic deformation (Fig. 5d). It is known that crystalline polymers are stiffer than amorphous ones. On the other hand, crystalline polymers are more brittle and less ductile. Therefore, during the wear testing, a more amorphous polymer coating (more GN-containing coating in this case) is likely to be able to adjust to the stress of the test by deforming plastically, giving rise to the enhanced anti-wear performances. The impact of the GN content on the wear performance of the coatings is therefore also partially accomplished by its influence on the degree of crytallinity of the coatings. The special lamellar structure of the present thermal sprayed UHMWPE–GNs coatings should also take part in mediating the wear behavior of the coatings, which needs to be further explored.

The potentiodynamic polarization curves and Bode plots by impedance spectroscopy measurements of the coating samples

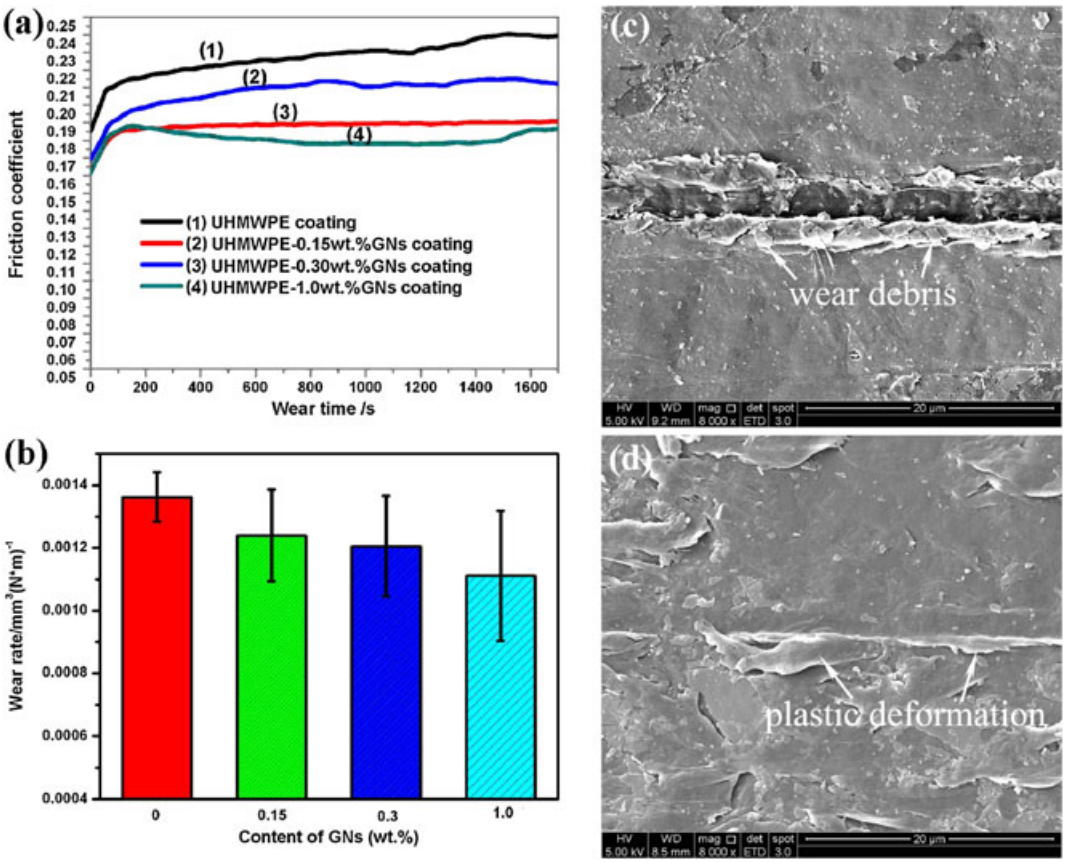

Figure 5. Wear properties and worn morphology of the coatings. Variations of friction coefficient (a) and wear rate (b) of the UHMWPE–GN coatings are influenced by the content of GNs in the coatings. The pure UHMWPE coating shows more plastic deformation along the wear scar (c), while the UHMWPE–1.0wt.%GN coating shows wear debris around the wear scar (d).

after immersion in 3.5 wt.% NaCl aqueous solution are shown in Fig. 6. It is clear that the GN-containing coatings yield higher corrosion potential (E_{corr}) values than the pure UHMWPE coating (Fig. 6a). Moreover, E_{corr} shifted to the direction of positive potential for the coatings with higher loading of GNs, −0.537 V for the coating without GNs, −0.466 V for the coating with 0.15 wt.% GNs, −0.439 V for the coating with 0.30 wt.% GNs, and −0.433 V for the coating with 1.0 wt.% GNs, suggesting enhanced anti-corrosion performance of UHMWPE by addition of GNs. Given that E_{corr} is the measure of corrosion susceptibility,[31] the shift in E_{corr} in the more positive direction is consistent with the earlier inferences of super corrosion resistance of graphene coating.[32] Corrosion current density and polarization resistance are often used as important parameters to evaluate the kinetics of corrosion reactions. Corrosion protection is normally proportional to corrosion current density (i_{corr}) as measured via polarization.[33] By examining i_{corr} value at the same polarized potentials, significant reduction in dissolution current as a result of addition of GNs has been observed (Fig. 6a). The higher content of GNs in the composite coatings corresponds to higher i_{corr} value, further evidencing markedly improved corrosion resistance by addition of GNs. The EIS measurement gives further information about the corrosion behavior of the coating samples under open-circuit condition (Fig. 6b). In using EIS for understanding electrochemical degradation of metals and their coated samples, the Bode and Nyquist plots are the most common representations of the processes occurring at various interfaces.[32] In this study, Bode plots have been selected as the primary representation of capability of the coatings of protecting the substrates from the corrosion. Z_{real} is a measure of corrosion resistance[34], and increased Z_{real} corresponds to better corrosion resistance.[35] In the case of Bode plots, the magnitude of the impedance at the lowest frequency also represents the corrosion resistance. The Bode plots of the EIS spectra for the coatings suggest positive effect of GN addition on Z_{real} values; 1.0 wt.% GN addition accomplished the highest Z_{real}. Graphene film alone has been revealed to be able to protect copper from electrochemical degradation by one and half orders of magnitude.[32] It is well accepted that impedance measurements provide information on both the resistive and capacitive behaviors of interface and make it possible to investigate the performance of a polymer coating as a protective layer against metal corrosion.[36] In general, the higher the value of corrosion potential is, the less likely the coating system tends to corrode. The superior performance of graphene as a filler, high specific surface area, two-dimensional sheet geometry, strong filler–matrix adhesion, and the outstanding mechanical properties of the sp2 carbon-bonding network are always responsible for the enhanced performances of the graphene-containing polymers. Yet, the mechanism behind the enhanced anti-corrosion performances remains obscure. As one of the key factors that are involved in tailoring the properties of the UHMWPE–GN coatings like anti-wear and corrosion performances, interfaces between UHMWPE and GNs leave a lot of uncertainties, substantially due to the difficulties in visualizing them. Presence of GNs at UHMWPE splats' interfaces has been observed (Fig. 1e,f), and strengthening effect by bridging was expected for the UHMWPE–GN coatings.

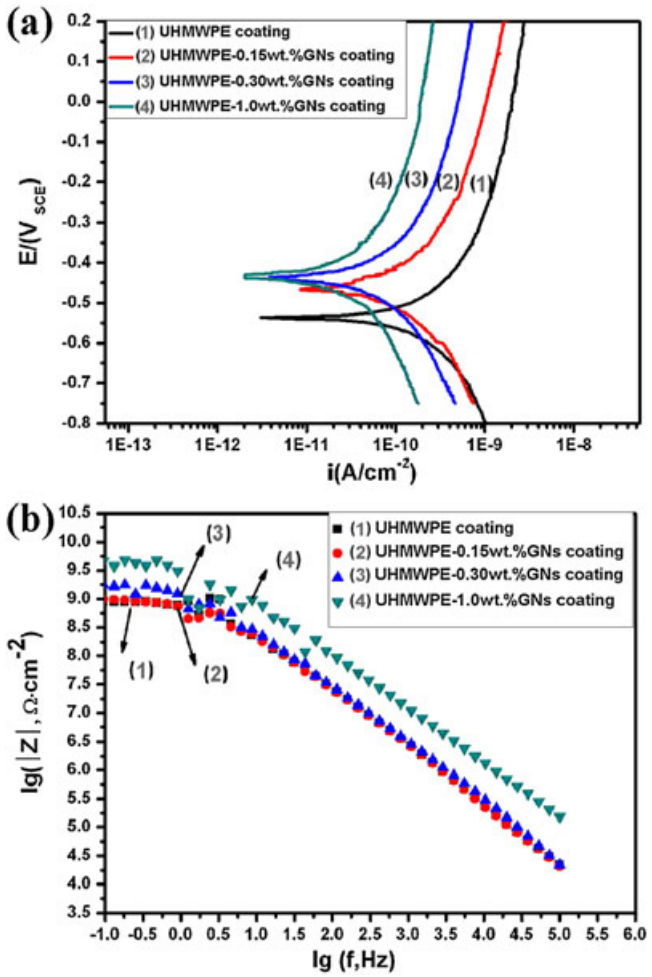

Figure 6. Potentiodynamic polarization curves (a) and electrochemical impedance spectroscopy measurement as Bode plot (b) for the UHMWPE–GN coatings.

Ongoing efforts by these authors through characterizing the UHMWPE–GN interface by transmission electron microscopy are expected to facilitate a more fundamental understanding of the effect of addition of GNs on the structure and properties of the flame sprayed UHMWPE-based coatings.

CONCLUSIONS

Novel UHMWPE–GN composite coatings have been successfully fabricated by flame spraying. The content of GNs was tailored in a range up to 1.0 wt.%. The UHMWPE–GN composites did not suffer detectable thermal degradation during the coating deposition. Addition of GNs resulted in increases in microhardness and enhanced anti-wear performance of the UHMWPE coatings, which is most likely attributed to the high toughness and wear resistance of graphene and the bridging effect achieved by GNs located at interfaces between UHMWPE splats. GNs retained their nanolayered structure and contribute to significantly reduced friction coefficient of the coatings (0.18 *versus* 0.24). In addition, incorporation of GNs gave rise to better corrosion resistance of the UHMWPE coatings. Further profound understanding of the influence exerted by GN addition on structure of UHMWPE in molten state and the interfaces between GNs and UHMWPE is to be explored.

Acknowledgement

This research was supported by 100 Talents Program of Chinese Academy of Sciences (to H.L.).

REFERENCES

[1] S. Li, *Oper. Techn. Orthopaedics* **2001**, *11*, 288–295.
[2] Y. Bao, T. Zhang, D. T. Gawne, *J. Mater. Sci.* **2005**, *40*, 77–85.
[3] K. Park, S. Mishra, G. Lewis, J. Losby, Z. F. Fan, J. B. Park, *Biomaterials* **2004**, *25*, 2427–2436.
[4] G. Lewis, *Biomaterials* **2001**, *22*, 371–401.
[5] M. Deng, S. W. Shalaby, *Biomaterials* **1997**, *18*, 645–655.
[6] T. M. Wright, D. J. Astion, M. Bansal, C. M. Rimnac, T. Green, J. N. Insall, R. P. Robinson, *J. Bone Joint Surg. Am.* **1998**, *70*, 926–932.
[7] L. M. Fang, P. Gao, Y. Leng, *Compos. Part B-Eng.* **2007**, *38*, 345–351.
[8] W. Tang, M. H. Santare, S. G. Advani, *Carbon* **2003**, *41*, 2779–2785.
[9] S. L. Ruan, P. Gao, X. G. Yang, T. X. Yu, *Polymer* **2003**, *44*, 5643–5654.
[10] H. J. Liu, D. Xie, L. M. Qian, X. R. Deng, Y. X. Leng, N. Huang, *Surf. Coat. Technol.* **2011**, *205*, 2697–2701.
[11] W. J. Wood, R. G. Maguire, W. H. Zhong, *Compos. Part B-Eng.* **2011**, *42*, 584–591.
[12] Z. X. Tai, Y. F. Chen, Y. F. An, X. B. Yan, Q. J. Xue, *Tribol. Lett.* **2012**, *46*, 55–63.
[13] S. Stankovich, D. A. Dikin, G. H. B. Dommett, K. M. Kohlhaas, E. J. Zimney, E. A. Stach, R. D. Piner, S. T. Nguyen, R. S. Ruoff, *Nature* **2006**, *442*, 282–286.
[14] J. R. Davis, *Handbook of thermal spray technology*. ASM International, Thermal Spray Society Training Committee, Materials Park, OH, **2004**.
[15] J. R. T. Branco, S. R. V. Campos, L. T. Duarte, V. F. C. Lins, *J. Appl. Polym. Sci.* **2004**, *92*, 3159–3166.
[16] L. T. Duarte, E. M. Paulae Silva, J. R. T. Branco, V. F. C. Lins, *Surf. Coat. Technol.* **2004**, *182*, 261–267.
[17] T. Palathai, J. Tharajak, N. Sombatsompop, *Mater. Sci. Eng. A* **2008**, *485*, 66–73.
[18] K. Patel, C. S. Doyle, B. J. James, M. M. Hyland, *Polym. Degrad. Stabil.* **2010**, *95*, 792–797.
[19] K. Alamara, S. Saber-Samandari, C. C. Berndt, *Surf. Coat. Technol.* **2010**, *205*, 2518–2524.
[20] M. J. McAllister, J. L. Li, D. H. Adamson, H. C. Schniepp, A. A. Abdala, J. Liu, M. Herrera-Alonso, D. L. Milius, R. Car, R. K. Prud'homme, I. A. Aksay, *Chem. Mater.* **2007**, *19*, 4396–4404.
[21] X. W. Jiang, Y. Z. Bin, N. Kikyotani, M. Matsuo, *Polym. J.* **2006**, *38*, 419–431.
[22] P. Kim, L. Shi, A. Majumdar, P. L. McEuen, *Physica B* **2002**, *323*, 67–70.
[23] K. E. Prasad, B. Das, U. Maitra, U. Ramamurty, C. N. R. Rao, *Proc. Natl. Acad. Sci. USA* **2009**, *106*, 13186–13189.
[24] J. J. Liang, Y. Huang, L. Zhang, Y. Wang, Y. F. Ma, T. Y. Guo, Y. S. Chen, *Adv. Funct. Mater.* **2009**, *19*, 2297–2302.
[25] H. J. Salavagione, G. Martinez, M. A. Gomez, *J. Mater. Chem.* **2009**, *19*, 5027–5032.
[26] R. Verdejo, M. M. Bernal, L. J. Romasanta, M. A. Lopez-Manchado, *J. Mater. Chem.* **2011**, *21*, 3301–3310.
[27] L. S. Shi, L. Y. Wang, Y. N. Wang, *Eur. Polym. J.* **2006**, *42*, 1625–1633.
[28] M. R. Sanchis, V. Blanes, M. Blanes, D. Garcia, R. Balart, *Eur. Polym. J.* **2006**, *42*, 1558–1568.
[29] T. Kuila, S. Bose, C. E. Hong, M. E. Uddin, P. Khanra, N. H. Kim, J. H. Lee, *Carbon* **2011**, *49*, 1033–1037.
[30] D. L. Burris, B. Boesl, G. R. Bourne, W. G. Sawyer, *Macromol. Mater. Eng.* **2007**, *292*, 387–402.
[31] D. A. Jones, *Principles and prevention of corrosion*, 2nd edn. Prentice Hall, NJ, USA, **1996**.
[32] R. K. S. Raman, P. C. Banerjee, D. E. Lobo, H. Gullapalli, M. Sumandasa, A. Kumar, L. Choudhary, R. Tkacz, P. M. Ajayan, M. Majumder, *Carbon* **2012**, *50*, 4040–4045.
[33] D. K. Merla, P. Panjan, M. Cekada, M. Macek, *Electrochim. Acta* **2004**, *49*, 1527–1533.
[34] F. Zucchi, V. Grassi, A. Frignani, C. Monticelli, G. Trabanelli, *J. Appl. Electrochem.* **2006**, *36*, 195–204.
[35] M. A. Arenas, T. J. Tate, A. Conde, J. de Damborenea, *Brit. Corros. J.* **2000**, *35*, 232–236.
[36] S. L. A. Maranhao, I. C. Guedes, F. J. Anaissi, H. E. Toma, I. V. Aoki, *Electrochim. Acta* **2006**, *52*. 519–526.